View metadata, citation and similar papers at core.ac.uk
brought to you by CORE
provided by Elsevier - Publisher Connector

ELSEVIER

Available online at www.sciencedirect.com

SciVerse ScienceDirect

Physics Procedia 39 (2012) 650 – 660

Physics Procedia

LANE 2012

Advances in ultra short pulse laser based parallel processing using a spatial light modulator

G. Dearden*, Z. Kuang, D. Liu, W. Perrie, S.P. Edwardson, K.G. Watkins

Laser Group, Centre for Materials and Structures, School of Engineering, University of Liverpool, L69 3GQ, UK

- Invited Paper -

Abstract

Presented here are latest advances in ultra short pulse laser based parallel processing using a spatial light modulator (SLM), which has the potential for use in high throughput precision patterning of photovoltaic and other device layers. Ultra short laser pulses allow selective material removal with minimal energy density, while here a computer-generated hologram driven reflective SLM is used to transform a single beam into multiple beamlets for increased process throughput. Based on this technique, the precision patterning of silicon, titanium, thin film ITO and metal on flexible and glass substrates is demonstrated and the benefits and current limitations discussed.

© 2012 Published by Elsevier B.V. Selection and/or review under responsibility of Bayerisches Laserzentrum GmbH
Open access under CC BY-NC-ND license.
Keywords: ultra short pulse laser; laser ablation; laser patterning; parallel processing; spatial light modulator

1. Introduction

Laser patterning is a key industrial process for use in the manufacture of photovoltaic devices such as organic light emitting diode (OLED) displays, solid-state lighting foils and solar cells. Ultra short pulse lasers are of particular interest as they may enable selective ablative removal of material layers with minimal energy density, hence avoiding damage or unwanted effect to adjacent layers. Since the output pulse energy of commercial laser sources currently far exceeds that required for single beam processing, parallel processing with multiple beams could provide a novel route for scaling up process throughput and reducing manufacturing costs. The approach discussed here uses a reflective liquid crystal on silicon

* Corresponding author. Tel.: +44 151 794 4584.
E-mail address: g.dearden@liv.ac.uk.

1875-3892 © 2012 Published by Elsevier B.V. Selection and/or review under responsibility of Bayerisches Laserzentrum GmbH
Open access under CC BY-NC-ND license. doi:10.1016/j.phpro.2012.10.085

spatial light modulator (SLM), driven by fast computer-generated holograms, to split a parent laser beam into a number of beamlets and digitally manipulate their position and intensity on or over the target area.

Spatial Light Modulators (SLMs) are adaptive optical devices that can modulate the properties of an incoming optical wavefront, such as phase, amplitude or polarisation. Since their introduction in the 1980's [1], SLMs have attracted increasing attention in many research areas that include temporal pulse shaping [2], holographic optical tweezers [3, 4], wavefront correction [5, 6], spatial beam shaping [7, 8] and laser parallel processing [9-11]. A common implementation of a SLM is the liquid crystal (LC)-based SLM. The basic principle of operation of these devices is that the phase change of the light polarized along the crystal's extraordinary axis can be precisely controlled by the variable refractive index of LC materials. Since LC-based SLMs usually modulate light in response to either optical or electrical inputs, they can be classified as two major categories: namely, optically and electrically addressed SLMs. An optically addressed SLM (or optically addressed light valve), which is constructed of a continuous photosensitive layer on top of modulating material, has the ability to modulate a light beam using another beam; however, its manufacturing cost is relatively high. On the other hand, an electrically addressed SLM comprises a pixelated structure that is manipulated electrically so as to modulate the local optical wavefront at each individual pixel. The advantage of this device type is the capability of direct interfacing between optical and electronic units. However, its drawbacks are the lower light utilization efficiency (owing to the dead zone between the electrodes) and diffraction losses caused by the pixelated structure.

Parallel processing using diffractive multiple beams generated by a SLM has been shown to increase the throughput and efficiency of ultra short pulse laser processing. By synchronisation with a scanning galvanometer, further flexibility in micromachining has been demonstrated [9-12]. Since many industrial applications would require that all the diffractive beams have a good identity to ensure a consistent processing, the uniformity of the diffractive pattern is a significant parameter. As reported by Curtis et al [13], the uniformity of the diffractive pattern is not only affected by the algorithm used to calculate CGH [14, 15], but also the geometric design of the diffractive pattern. A slight spatial disordering of periodic and symmetric patterns can significantly reduce intensity variations among each of the desired diffractive peaks. In the literature, a better uniformity of diffractive pattern has been demonstrated by improving the CGH calculation algorithm, e.g. adding iterative calculations to minimize the uniformity error of the computationally reconstructed diffractive peaks [16, 17], or by taking account of the intensity distribution of the irradiated laser pulse and the spatial frequency response of the SLM [16, 19-20]. However, there has been little work studying experimentally the effect of different geometric designs of diffractive pattern uniformity. In this paper, multiple laser beams parallel processing including selective ablation and large-area processing are demonstrated. In addition, beam shaping with an SLM is also presented. A study into the effect on uniformity of varying the geometric pattern design is also given.

2. Experimental

The ultra short pulse laser system used for the present research was a custom made Nd:VAN seeded regenerative amplifier (High-Q IC-355-800ps, Photonics Solutions). Figure 1 shows the schematic of the experimental setup. The output laser beam (t_p = 10ps, λ = 1064nm) passed through a half wave plate used for adjusting the linear polarization direction, a beam expander (M $\approx \times 3$) and, after reflection on mirrors 1, 2 and 3, illuminated a reflective SLM oriented at <10 degree angle of incidence. A 4f-optical system was formed from A to D to remove the unwanted 0-th order beam. The modulated beam then entered a scanning galvanometer with f = 100mm flat field of f-theta lens (Nutfield), providing an agile focusing system. Substrates were mounted on a precision 5-axis (x, y, z, p, q) motion control system (Aerotech)

allowing accurate positioning of the substrate surface at the laser focus. The spectral bandwidth, $\Delta\lambda \approx$ 0.1nm, was relatively narrow and important in eliminating chromatic dispersion of the SLM [3].

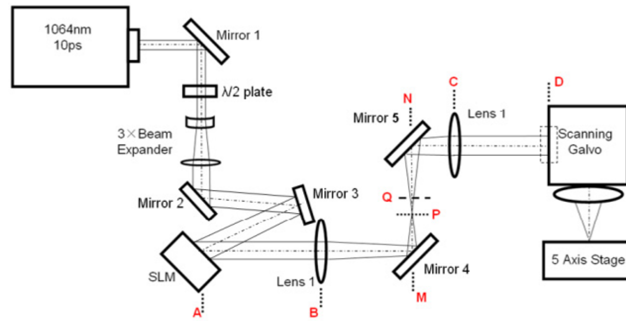

Fig. 1. Schematic of experiment setup for High-Q IC-355-800ps with a 4f optical system

Two different SLMs (Hamamatsu X10468-04 and Holoeye LC-R2500) were used in the experiments. These are both pixelated electrically addressed reflective SLMs and the specifications of the devices are listed in Table 1. The X10468 has a dielectric mirror, which provides 95% light utilization efficiency but is only usable over a specified wavelength range. Whereas, the LC-R2500 has a metal coated mirror that offers lower light utilization efficiency (~75%), but covers a wide wavelength range from visible to near infrared (NIR). The phase modulation of the LC-R2500 did not reach 2π when used at a wavelength of 1064 nm, but this had negligible effect in the experiments. Applying a voltage to the X10468 (a parallel aligned nematic crystal device) resulted in the LC molecules aligning horizontally along the optical axis, hence changing the phase of light polarised along the molecular axis, but leaving completely unaffected light polarised perpendicular to the molecular axis. Contrastingly, the LC-R2500 has a 45° twisted nematic LC layer in which the LC molecules are arranged in a twisted array from the front to the back. This kind of device can not only modulate the phase of light, but also rotate the plane of polarization.

Table 1. Specifications of SLMs

Model	Hamamatsu X10468-04	Holoeye LC-R2500
LC Type	Parallel-aligned nematic	45° twisted nematic
Model	Phase only	Phase & Amplitude
Resolution (pixels)	SVGA(800×600)	XGA(1024×768)
Pixel pitch (μm)	20	19
Effective area (mm^2)	16×12	19.5×14.6
Mirror coating	Dielectric	Broadband metallic
Readout wavelength (nm)	510±50	400~1064
Reflectivity	95%	~75%*
Fill Factor	95%	93%
Response time** (rise/fall ms)	15/30	10/18
Frame rate (Hz)	60	72

* The actual reflectivity depends on readout light wavelength.
**The time required to change from 10 % to 90 % for 2π modulation.

To generate high quality fast computer-generated holograms (CGHs), the use of non-iterative Lenses and Gratings (LG) [14], iterative Fourier transform based Gerchberg-Saxton (GS) and weighted Gerchberg-Saxton (GSW) algorithms [21] was carried out within a LabView environment [22].

A periodic 5×5 array with high degree of symmetry (figure 2 (a)), was the basic geometric design of diffractive pattern. To quantitatively control the degree of symmetry, each of the diffracted beamlets in the pattern was assigned a freedom of asymmetry (R); hence, they no longer had a fixed position but were located randomly within a circle area (centre: (ρ_i, ρ_j); Radius = R), as depicted in figure 2 (b).

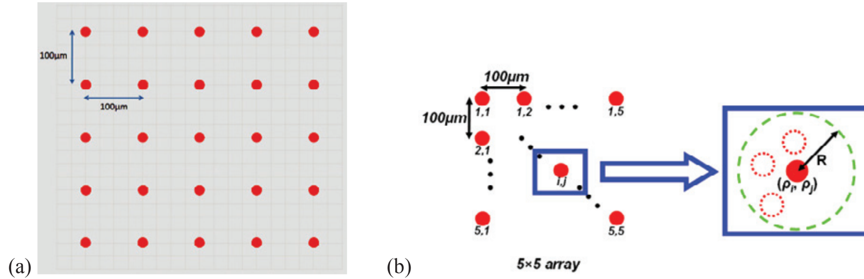

Fig. 2. (a) The periodic 5×5 array with high degree of symmetry - the basic geometric design of a diffractive pattern. (b) Schematic showing the position of each desired diffractive peaks randomly located within a circle area, due to the freedom of asymmetry – R

The uniformity of the diffractive patterns can be quantitatively described by calculating the standard deviation, σ. In this study, the diameter of each micro-sized hole machined by the diffracted beams, D_1, D_2, D_3 ... D_n, was firstly measured, and then an average value ($\overline{D}$) was calculated from:

$$\overline{D} = \frac{1}{n}\sum_{i=1}^{n} D_i \tag{1}$$

Accordingly, the standard deviation was calculated from:

$$\sigma = \sqrt{\frac{1}{n}\sum_{i=1}^{n}(D_i - \overline{D})^2} \tag{2}$$

Finally, the percentage variation was analysed to quantitatively describe the uniformity of diffracted beams according to the following calculation.

$$V = \frac{\sigma}{\overline{D}} \times 100\% \tag{3}$$

Different materials such as silicon, Ti6Al4V, OLED cathode (Aluminium) and Indium Tin Oxide (ITO) thin film (60 nm thick) on glass were employed in the experiments.

3. Results and Discussion

3.1. Uniformity study of diffractive multi-beam patterns

The optical micrographs in figure 3 demonstrate the machining results on a polished Ti6Al4V substrate using the LG algorithm. The effect on pattern uniformity of varying the freedom of asymmetry can be observed. Patterns with a high degree of symmetry showed poor uniformity, e.g. when R =2 µm, V ≈ 41.2%, while asymmetrically designed pattern has a good uniformity, e.g. when R =50 µm, V ≈ 5.6%.

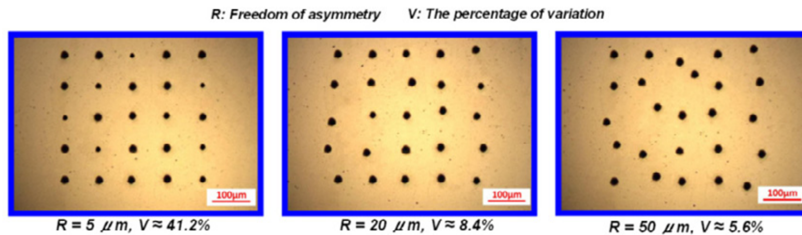

Fig. 3. Optical micrographs demonstrating the machining results on a polished Ti6Al4V substrate using LG algorithm, when the freedom of asymmetry (R) was set to be 2 µm, 20 µm and 50 µm

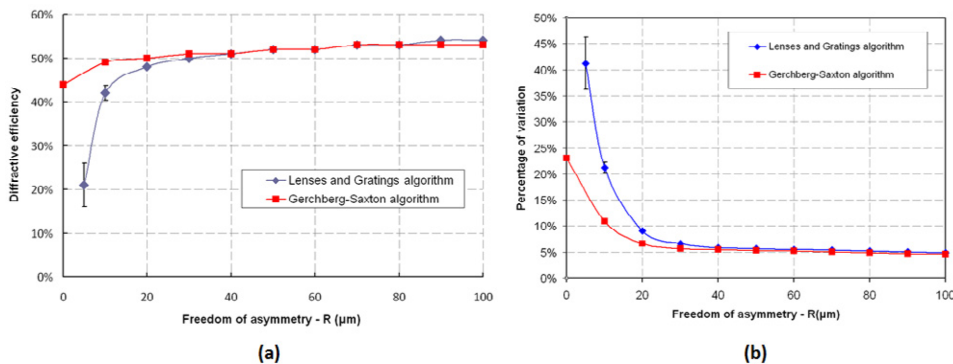

Fig. 4. (a) the diffraction efficiency versus the freedom of asymmetry, R; (b) the uniformity, described by the Percentage of Variation, versus the freedom of asymmetry, R

The results in figure 4 show the measured diffraction efficiency (a), the total fraction of light directed to the desired multiple beams, and uniformity (b) versus the freedom of asymmetry, R, where the applied CGHs were calculated using two different algorithms, Lenses and Gratings (LG) and Gerchberg-Saxton (GS). Each data point in the figures represents the average value calculated from five different random patterns given the same freedom of asymmetry, R. As shown in the graphs in figure 4, the asymmetrically designed geometric pattern (R > 20µm) greatly improves the uniformity and diffraction efficiency. For symmetric patterns (R < 20µm), the iterative GS algorithm clearly outperforms the LG algorithm. Nonetheless, by increasing of the freedom of asymmetry (R), both uniformity and diffraction efficiency were greatly improved using the LG algorithm, reached the quality using the GS algorithm.

3.2. The degeneracy of the design pattern

Unwanted diffractive intensity peaks may be generated with the desired multiple beams. These peaks are sometimes called ghosts in literature. A simple example of ghosts is the higher-order diffraction peaks produced by a phase grating. This grating, equivalent to a prism, deflects a +1 order beam to a position (ρ_x, ρ_y) by imposing the phase $\varphi \propto \rho \bullet r$, where r is the hologram coordinate. The weaker higher-order beams also appear in predictable positions, as shown in figure 5 (a).

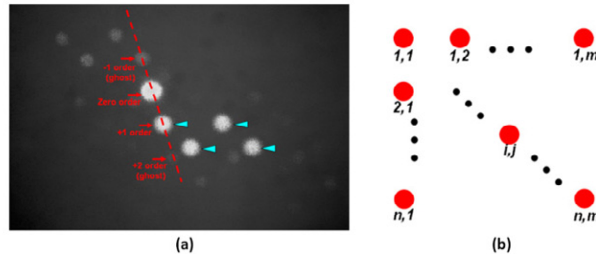

Fig. 5. (a) A digital camera photo showing a diffractive pattern reconstructed on a paper screen – Only the triangle marked four brighter spots are the desired diffractive orders, all the other weaker spots appeared on the dark background are ghosts. The red dashed line marks a series spots generated by a phase grating, where only the +1 order is desired. (b) N×M beams array

With the Lenses and Gratings (LG) algorithm, a CGH which can generate the N×M beam array shown in figure 5 (b), is represented as:

$$\varphi_h = \sum_{i,j}^{n,m} \varphi_{i,j} \tag{4}$$

where, $\varphi_{i,j}$ is a phase of prism which can deflect a +1 order beam to the desired position, (ρ_i, ρ_j).

Without giving a sufficient extra freedom to avoid the degeneracy caused by the ghosts overlapping and interfering with the desired orders [13], the highly symmetric patterns can end up with a high degree of non-uniformity and poor diffraction efficiency, explaining the results in figures 3 and 4 when R < 10 with the LG algorithm. On applying a freedom of asymmetry R, the position of each designed +1 order beams was no longer fixed, but randomly located within a circle area (centre: (ρ_i, ρ_j); Radium = R), as shown in figure 2 (b). In this way, a random phase, $\varphi_{i,j\,(R)}$, was added to the individual $\varphi_{i,j}' = \varphi_{i,j} + \varphi_{i,j(R)}$ prism phase. The phase CGH for the pattern with R can then be represented as:

$$\varphi_h' = \sum_{i,j}^{n,m} \varphi_{i,j}' = \sum_{i,j}^{n,m} (\varphi_{i,j} + \varphi_{i,j(R)}) \tag{5}$$

Thus, R is equivalent to adding an extra phase (ϕ i,j (R)), which gave the extra freedom to improve the uniformity of the diffractive pattern by decreasing the possibility of degeneracy. The larger the value of R, the more freedom of phase was delivered to each of the desired +1 order beams, hence further avoiding the degeneracy, which explains the results shown in figure 4.

3.3. Multiple beam parallel processing

The symmetry of multiple beams can greatly affect the intensity distribution across all beams [13]. Figure 6 (a) shows a common multi-beam pattern with perfect symmetry for parallel processing, however, the symmetric pattern suffers from low intensity uniformity even using iterative algorithm like GS (~60%) [15]. One approach to solve this problem is to introduce a small amount of random displacement to the multi-beam pattern, since for most algorithms spatial randomization can significantly reduce intensity variation [13]. Another method is to use the GSW algorithm, which can obtain >90% uniformity even with a symmetric pattern. However, the calculation speed of GSW is slower than that of GS. Here, the first method was adopted. The beams were slightly misaligned in the Y direction, but kept the same separation _ in the Z direction, as shown in figure 6 (b), to optimize energy distribution across the array.

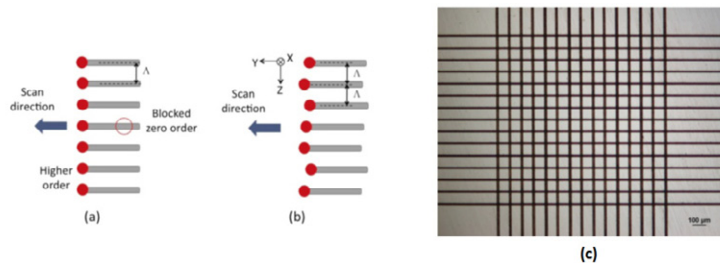

Fig. 6. Schematics of (a) a symmetric multi-beam pattern and (b) an asymmetric multi-beam pattern for parallel processing; (c) Optical micrograph of silicon sample processed with 15 parallel beams

Figure 6 (c) shows a micrograph of the silicon sample that was scribed using 15 asymmetric beams, as depicted in figure 6 (b), produced using the X10468-4 SLM at a wavelength of 532 nm, 10ps pulse length and 5kHz repetition rate. The 15 beams with total incident pulse energy of 21 μJ (1.4 μJ/pulse/beam) were scanned orthogonally with two CGHs at 10 mm/s to produce the cross-hatched pattern. The scribe lines were measured to be ~ 500 nm deep and 14 μm wide, while the pitch Λ was 86 μm. Adjusting the CGH could control the pitch Λ, while applying lower laser pulse energies reduced the scribe width. There was no observed thermal damage to the surrounding area.

3.4. Cathode patterning of OLEDs

OLEDs are multi-layer materials, with each layer having its own particular ablation threshold. For example, the top cathode layer (aluminium) has a lower ablation threshold than the underlying anode layer (ITO film), hence selective removal of the aluminium can be achieved by controlling the laser fluence. Figure 7 (a) and (b) show respectively a micrograph and optical surface profile of a cross hatch patterned OLED layer produced by 15 beams from the X10468-04 SLM at 532 nm wavelength. The laser pulse energy, pulse repetition rate and scanning speed were 12 μJ, 5 kHz and 30 mm/s, respectively.

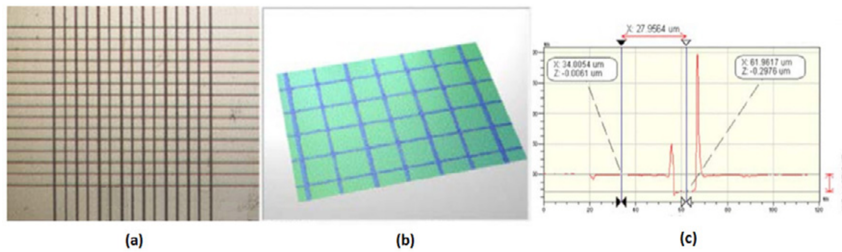

Fig. 7. Parallel processing of OLED using 15 beams. (a) Optical micrographs; (b) 3D surface profile; (c) Cross-sectional profile of a single line

Only a single scan of the array was required tp produce multiple scribe lines with a pitch of 86 µm, line widths of ~10 µm and depths of ~ 290 nm. Each scribe line, as seen in figure 7 (c), showed a flat bottom area indicating that the cathode and organic layers were removed, while the underlying (ITO film) anode remained unaffected. Optimisation of process parameters could further improve this structuring.

3.5. Selective ablation using multiple spots per line

Beam scanning with different numbers of spots per line can mimic a variable spot overlap and produce controllable ablation depth. For the example shown in figure 8 (a), (b) and (c), 10 beamlets were arranged in a 4-3-2-1 pattern to achieve selective scribing of silicon at different positions in a single scan (the red dots denoting the beam pattern used). The total pulse energy incident on the sample was 18 µJ, giving 1.8 µJ per beam. For a wavelength of 532 nm, repetition rate of 5 kHz and scan speed of 1 mm/s the 4-3-2-1 spot array produced scribe lines with depths of ~2.82, 1.81, 1.33 and 0.82 µm respectively. The method enables highly flexible control of the number of beams and the location, pitch and depth of scribe lines.

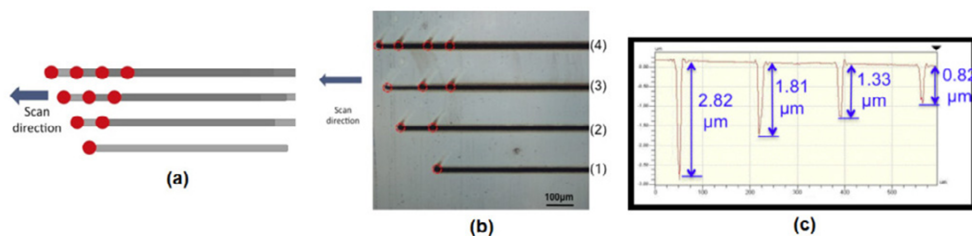

Fig. 8. (a) Schematic of selective ablation using different numbers of spots per line; (b) Micrograph of selective ablation on silicon. The red circles represent the positions of the 10 beams; (c) Cross-sectional surface profile of selective ablation on silicon

3.6. Large area processing

In some applications, such as thin film removal, a specific size or shape of line focus is required for processing a large area. For such applications, multiple beamlets of a particular arrangement for parallel processing were found to produce similar results to scanning with a specially shaped beam, as depicted in figure 9 (a). Figure 9 (b) shows the result of 40 beams processing in parallel a silicon sample using a pulse energy ~1.75 µJ/pulse/beam, a repetition rate of 5 kHz, a scan speed of 1 mm/s and one over scan.

These parameters produced an ablated region 457.6 μm wide and 5 μm deep. The GSW algorithm was used to calculate the CGH, because a symmetric pattern was required. Since the width of ablated region could be adjusted by simply changing the number of spots, this method provides high potential flexibility.

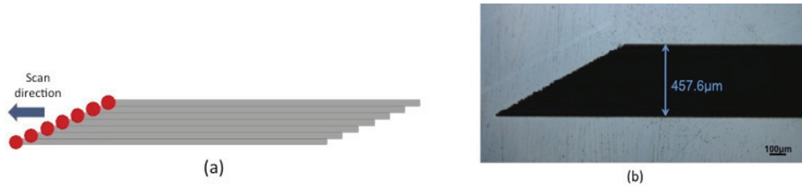

Fig. 9. Multi-beam large area processing: (a) Schematic diagram; (b) Processing of silicon at 532nm with 40 parallel beams

3.7. Beam Shaping - Annular beam case

Annular beams, generated by an LC-R 2500 SLM using diffractive axicon holograms at 1064nm, were used to ablate ITO thin film on a glass substrate. The radii of annular beams were controlled by adjusting the spatial frequency of the holograms. Patterning using a CGH with a higher spatial frequency of 1.67 line pairs/mm produced a ring with r = 174 μm; while with lower spatial frequency 0.83 line pairs/mm CGH, a ring with r = 90 μm was marked. The pulse energies used were 129 μJ and 75 μJ respectively. A slight curvature of the LC on silicon SLM would result in slightly asymmetric rings, but this effect could be eliminated by applying a suitable distortion correction pattern to the SLM during the processing.

3.8. Parallel surface micro-structuring of ITO coated glass

Surface micro-structuring of an ITO coated glass was investigated by parallel processing [22] with diffracted beams (t_p = 10ps, λ = 1064nm). The LG algorithm was used to calculate CGHs to generate a 25 beam array. The geometric design of the beam pattern and the scanning method used are shown in figure 10 (a), for the case of a a periodic 25×1 array design pattern (25 beams arranged in Y and 1 beam in X, shown as pattern 0). Each of the beamlets was given a freedom of asymmetry (R) in X direction. R = 5μm was set in Pattern A (highly symmetric) and R = 50μm was set in Pattern B (asymmetric). The patterns A and B were individually scanned in X at a speed of 20mm/s on the ITO coated glass sample to create micro-channels. The input pulse energy on SLM was approximately 50μJ with 5 kHz repetition rate.

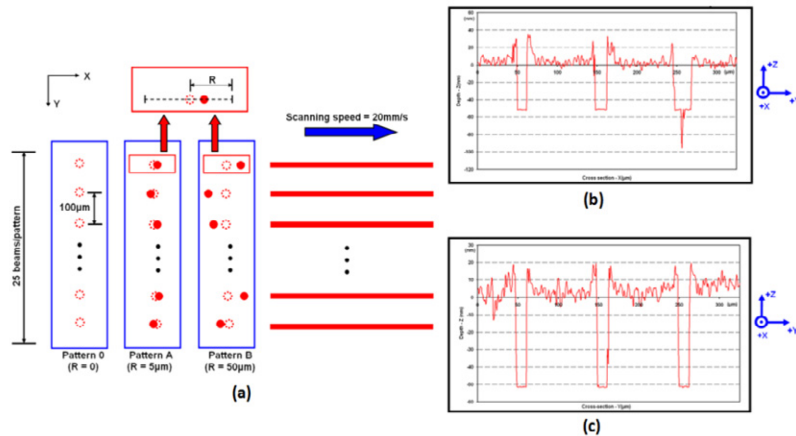

Fig. 10. (a) geometric beam pattern design and scanning method for surface micro-structuring of ITO coated glass; (b) machining results with the symmetric pattern A; (c) machining results with the asymmetric pattern B

The results of machining by patterns A and B are shown in figures 10 (b) and (c) respectively, where the cross section profile (observed by Wyko NT1100 optical surface profiler) showed that machining with the symmetric pattern A gave poor uniformity of structured channel width D_A (percentage of variation $V \approx 45.1\%$). The unequal diffraction meant that some of the diffracted beams had just enough energy to ablate the ITO coating, while the energy in others was sufficient to damage the glass substrate. The diffraction efficiency was measured to be only ~ 27%. In contrast, the asymmetric pattern B gave rise to structured micro-channels with good uniformity ($V \approx 5.3\%$), and the ITO coating was removed without damage to the glass substrate. The diffraction efficiency in this case was measured to be ~ 52%.

4. Conclusions

Advances made in ultra short pulse laser based parallel processing using a spatial light modulator discussed in this paper have demonstrated possible routes towards achieving high throughput, flexible and precise processing of materials at industrial scales. The benefits and limitations of the methods have been discussed. The results show that, to ensure a good uniformity of the diffracted beams, a highly symmetric pattern design should be avoided. Simple and computationally fast non-iterative algorithms can generate asymmetric patterns with excellent uniformity and high diffraction efficiency. Future work will address optimisation of CGH calculation and processing at high average powers via SLM design modification.

Acknowledgements

The authors gratefully acknowledge the support of the UK Technology Strategy Board, through project PARALASE.

References

[1] Efron, U.: *System Sciences* 1989; **1**: pp. 416-423.

[2] Weiner, A.M.; Leaird, D.E.; Patel, J.S; Wullert, J.R.: *Opt. Lett.* 1990; **15**: pp.326-8.

[3] Sun, B.; Roichman, Y.; Grier, D.G.: *Opt. Express* 2008; **16**: pp.15765-15776.

[4] Grieve, J.A.; Ulcinas, A.; Subramanian, S.; Gibson, G.M.; Padgett, M.J.; Carberry, D.M. et al: *Opt. Express* 2009; **17**: pp.3595-3602.

[5] Sanner, N.; Huot, N.; Audouard, E.; Larat, C.; Laporte, P.; Huignard, J.-P.: *Appl. Phys. B* 2005; **80**: pp. 27.

[6] Hu, L.; Xuan, L.; Liu, Y.; Cao, Z.; Li, D.; Mu, Q.: *Opt. Express* 2004; **12**: pp.6403-9.

[7] Sanner, N.; Huot, N.; Audouard, E.; Larat, C.; Huignard, J.P.: *Opt. and Las. in Eng.* 2007; **45**: pp.737–741.

[8] Sanner, N.; Huot, N.; Audouard, E.: *Opt. Lett.* 2005; **30**: pp.1479-1481.

[9] Kuang, Z.; et al: *Applied Surface Science* 2008; **255**: pp. 2284–9.

[10] Kuang, Z.; Liu, D.; Perrie, W.; Edwardson, S.P.; Sharp, M.; Dearden, G. et al: *Appl. Surface Science* 2009; **255**: pp. 6582-8.

[11] Kuang, Z.; Perrie, W.; Liu, D.; Edwardson, S.P.; Cheng, J.; Dearden, G. et al: *Appl. Surface Science* 2009; **255**: pp.9040-4.

[12] Kuang, Z.; Liu, D.; Perrie, W.; Cheng, J.; Shang, S.; Edwardson, S.P.; et al: *Chinese Journal of Lasers* 2009; **36** (12): pp.3093-3115.

[13] Curtis, J. E.; Schmitz, C.H.J.; Spatz, J.P.: *Optics Letters* 2005; **30**: pp. 2086-8.

[14] Leach, J.; Wulff, K.; Sinclair, G.; Jordan, P.; Courtial, J.; Thomson; L.; et al: *Applied Optics* 2006; **45**: pp. 897–903.

[15] Di Leonardo, R.; Ianni, F; Ruocco, G: *Optics Express* 2007; **15**: pp. 1913-1922.

[16] Hasegawa, S.; Hayasaki, Y.; Nishida, N.; *Optics Letters* 2006; **31**,: pp.1705-7.

[17] Leach, J.; Wulff, K.; Sinclair, G.; Jordan, P.; Courtial, J.; Thomson, L.; et al: *Applied Optics* 2006; **45**: pp. 897–903.

[18] Takahashi, H.; Hasegawa, S.; Hayasaki, Y.: *Applied Optics* 2007; **46**: pp.5917–5923.

[19] Chaen, K., Takahashi, H.; Hasegawa, S.; Hayasaki, Y.: *Optics Communiations* 2007; **280**: pp.165–172.

[20] Liesener, J.; Reicherter, M.; Haist, T.; Tiziani, H.J.: *Optics Communications* 2000; **185**: pp.77–82.

[21] Gerchberg, R.W.; Saxton, W.O.: *Optik* 1972; **35**: pp. 237-246.

[22] Kuang, Z.; Perrie, W.; Liu, D.; Fitzsimons, P.; Edwardson, S.P.; Fearon, E.; et al: *Applied Surface Science* 2012; **258**: pp.7601-6.